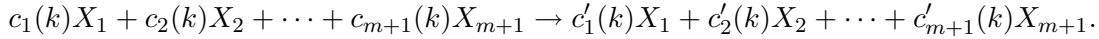


Supporting Information

S0. Discrete Chemical Master Equation

Here we first discuss the chemical master equation on a discrete state space. The CME describes the gain and loss of probability associated with each microstate due to chemical reactions. The chemical reactions can be thought as jump processes that bring the system from one combination of copy number of molecular species (micro state) to a different combination of copy number of molecular species once a reaction occurs. The CME describes the change of probability of different microstates connected by such jump processes due to reactions.

Specifically, we assume a system with $m + 1$ molecular species $\{X_1, \dots, X_{m+1}\}$, where X_i is the label of the i -th molecular species, and have n chemical reactions $\mathcal{R} = \{R_1, \dots, R_n\}$. We denote the copy number of the i -th molecular species as x_i . The combination of the copy numbers at time t is a vector of integers and is denoted as $\mathbf{x}(t) = (x_1(t), \dots, x_{m+1}(t)) \in \mathbb{N}^{m+1}$. We call $\mathbf{x}(t)$ the *microstate* of the system at time t . The probability for the system to be in state $\mathbf{x}(t)$ is $\mathbf{P}(\mathbf{x}, t)$. The set \mathcal{X} of all possible combinations of copy numbers $\mathcal{X} = \{\mathbf{x}(t) | t \in (0, \infty)\}$ is the *state space* of the system. Its size is denoted as $|\mathcal{X}|$. The collection of probabilities for each of the microstate at time t is the *probability landscape* $\mathbf{P}(t)$. Suppose a chemical reaction r_k has the form:



It brings the system from the microstate \mathbf{x}_j to \mathbf{x}_i . The difference between \mathbf{x}_j and \mathbf{x}_i is the stoichiometry vector \mathbf{r}_k of reaction k :

$$\mathbf{r}_k = \mathbf{x}_i - \mathbf{x}_j = (c_1(k) - c'_1(k), \dots, c_{m+1}(k) - c'_{m+1}(k)). \quad (1)$$

Here \mathbf{r}_k can admit 0 entries if a molecular species does not participate in the reaction, so \mathbf{r}_k has the same dimension as that of the microstate.

The rate of the k -th reaction that connects state \mathbf{x}_j to state \mathbf{x}_i is determined by the intrinsic reaction rate constant r_k , and the copy numbers of relevant reactants, which is given by the state \mathbf{x}_j :

$$A_k(\mathbf{x}_i, \mathbf{x}_j) = A_k(\cdot, \mathbf{x}_j) = A_k(\mathbf{x}_j) = r_k \prod_{l=1}^{m+1} \binom{x_l}{c_l}, \quad (2)$$

assuming the convention $\binom{0}{0} = 1$. If the k -th reaction can lead the system from state \mathbf{x}_j to state \mathbf{x}_i , we have $A_k(\mathbf{x}_i, \mathbf{x}_j) > 0$, otherwise $A_k(\mathbf{x}_i, \mathbf{x}_j) = 0$. In most cases, only one reaction connects two microstates. However, since in principle more than one reaction may connect state j to state i , we have the overall reaction rate that brings the system from \mathbf{x}_j to \mathbf{x}_i as:

$$A(\mathbf{x}_i, \mathbf{x}_j) = \sum_{k \in \mathcal{R}} A_k(\mathbf{x}_i, \mathbf{x}_j).$$

where $A(\mathbf{x}_i, \mathbf{x}_j)$ represents the transition probability function per unit time from \mathbf{x}_j to \mathbf{x}_i .

The discrete chemical master equation can then be written as:

$$\frac{d\mathbf{P}(\mathbf{x}, t)}{dt} = \sum_{\mathbf{x}'} [A(\mathbf{x}, \mathbf{x}')\mathbf{P}(\mathbf{x}', t) - A(\mathbf{x}', \mathbf{x})\mathbf{P}(\mathbf{x}, t)] \quad (3)$$

with $\mathbf{x}' \neq \mathbf{x}$. Note here we regard the probability $\mathbf{P}(\mathbf{x}, t)$ of a microstate is continuous in time, while the states are all discrete. The CME in this form fully account for the probabilities of jumps between states, regardless whether the copy number components of \mathbf{x}_i and \mathbf{x}_j are small or large. It gives a full account for the stochasticity due to small copy number events.

In Eqn. (3), the rate constant for leaving the current state $A(\mathbf{x}, \mathbf{x})$ does not appear. If we define

$$A(\mathbf{x}, \mathbf{x}) = - \sum_{\mathbf{x}', \mathbf{x}' \neq \mathbf{x}} A(\mathbf{x}', \mathbf{x}),$$

Eqn. (3) can be written in a more compact form:

$$\frac{d\mathbf{P}(\mathbf{x}, t)}{dt} = \mathbf{A}\mathbf{P}(\mathbf{x}, t), \quad (4)$$

where $\mathbf{A} \in \mathbb{R}^{|\mathcal{X}| \times |\mathcal{X}|}$ is the rate matrix formed by the collection of all $A(\mathbf{x}_i, \mathbf{x}_j)$ s:

$$\mathbf{A} = ||A(\mathbf{x}_i, \mathbf{x}_j)||, \quad \mathbf{x}_i, \mathbf{x}_j \in \mathcal{X}.$$

If we treat the state space as continuous, that is, we assume the amount of a molecular species x_i is measured by a real value (such as concentration) instead of an integer (copy numbers), the vector $\mathbf{x}(t)$ becomes a real-valued vector $\mathbf{x}(t) \in \mathbb{R}^{m+1}$. We have the chemical master equation equivalent to Eqn. (3) on continuous state space as:

$$\frac{\partial \mathbf{P}(\mathbf{x}, t)}{\partial t} = \int_{\mathbf{x}'} [A(\mathbf{x}, \mathbf{x}')\mathbf{P}(\mathbf{x}', t) - A(\mathbf{x}', \mathbf{x})\mathbf{P}(\mathbf{x}, t)]d\mathbf{x}' \quad (5)$$

where the kernel $A(\mathbf{x}, \mathbf{x}')$ represents the transition probability function per unit time from \mathbf{x}' to \mathbf{x} . The CME in this form is equivalent to the Chapman-Kolmogorov equation frequently used to describe continuous Markov processes.

Remark. The continuous state space version of the CME requires a strong assumption. It is only appropriate if one can assume that the difference in the amount of molecules in neighboring states is infinitesimally small, which is valid only if the copy number of the molecular species in the system are much larger than 1, and larger than the changes in the numbers of molecules when a reaction occurs. The continuous CME therefore cannot be used when the total amount of molecules involved is very small, for example, in systems of single or a handful of particles. In these cases, the discrete CME should be used, as it does not contain any intrinsic singularity difficulties.

S1. Enumeration of Microstates of Biological Network

A major hurdle in studying systems using discrete CME is the characterization of the space of microstates. Here we briefly summarize the key elements of our optimal algorithm for state enumeration. We use a slightly different notation to conform with conventions in computer science. Details can be found in [6]. For a network with m molecular species and n reactions, we calculate all microstates that the network can reach starting from a given initial condition. We denote a network as $\mathbf{N} = (\mathbf{M}, \mathbf{R})$, which has $m + 1$ number of molecular species: $\mathbf{M} = (M_1, \dots, M_{m+1})$, and n reactions: $\mathbf{R} = \{R_1, \dots, R_n\}$. A buffer of finite capacity is used from which synthesis reactions can generate new molecules, and to which degradation reactions can deposit molecules removed from the network. A

microstate is a specific combination of copy numbers of all molecular species $\mathbf{s} = (c_1, \dots, c_m, c_{m+1})$. Here c_1, \dots, c_m are the copy numbers of molecular species $1, \dots, m$. c_{m+1} is the number of net new molecules that can still be synthesized at this microstate. A reaction in principle can involve an arbitrary number (≥ 1 and $\leq m$) of molecular species as reactants and/or products, with any arbitrary positive integer coefficient (*i.e.*, arbitrary stoichiometry). Synthesis reaction is allowed to occur only if the buffer capacity is not exhausted, namely, only if $c_{m+1} > 0$. The set of all possible microstates \mathbf{s} that can be reached from an initial condition following these rules constitute the state space \mathcal{X} of the system: $\mathcal{X} = \{\mathbf{s}\}$. The set of allowed transitions is $\mathbf{T} = \{t_{ij}\}$, in which t_{ij} maps the microstate \mathbf{s}_j before the reaction to the microstate \mathbf{s}_i after the reaction. The initial condition is given as: $\mathbf{s}^{t=0} = (c_1^0, c_2^0, \dots, c_m^0, c_{m+1}^0)$, where c_i^0 is the initial copy number of the i -th molecular species at time $t = 0$, and $c_{m+1}^0 = B$ is the predefined buffer capacity.

The algorithm for enumerating the state space is summarized as Algorithm 1. After initialization, it starts with the given initial microstate $\mathbf{s}^{t=0}$. Each reaction is then examined in turn to determine if this reaction can occur for the current microstate. If so, and if the buffer is not used up, the state that this reaction leads to is generated. If the newly generated state was never encountered before, we add it to our collection of states for the state space, and declare it as a new state. We repeat this for all new states, which is maintained by a stack data structure. This terminates when all new states are exhausted. Details can be found in [6].

Following the approach outlined in references [9, 23, 26], the transition coefficient $\{a_{ij}\}$ between two different microstates \mathbf{s}_j and \mathbf{s}_i connected by a reaction is calculated by multiplying the intrinsic rate of this reaction with the reaction order dependent combination number of copies of reactants in the “before” state (see reference [6] for more details).

S2. Calculation of Steady State Probability Landscape

Following Kachalo *et al* [14], we obtain the Markovian state transition matrix \mathbf{M} from the reaction rate matrix \mathbf{A} : $\mathbf{M} = \mathbf{I} + \mathbf{A} \cdot \Delta t$, where \mathbf{I} is the identity matrix, and Δt is the discrete time unit and is chosen to be 1. The steady state probability landscape over the microstates, namely, the probability distribution function \mathbf{P} of the microstates can be obtained by solving the equation

$$\mathbf{P} = \mathbf{M}\mathbf{P}.$$

Since the steady state distribution also corresponds to the eigenvector of \mathbf{M} with eigenvalue of 1, one can also use the Arnoldi method as implemented in the software ARPACK to compute the steady state distribution \mathbf{P} [18]. An alternative is to solve $\mathbf{A}\mathbf{P} = 0$ directly.

Note this probabilistic landscape is different from that of a previous study, in which the landscape is that of a potential function, where the two peaks and the transition saddle point exist simultaneously, with transition between lysogenic and lytic states described by a Kramers process [30].

S3. Calculations of CI_2 and Cro_2 levels

The steady state protein concentration of CI_2 and Cro_2 dimer are calculated from the landscape as: $C_m = \sum_{\mathbf{s} \in \mathcal{X}} \mathbf{P}(\mathbf{s}) s_m$, $m \in \{\text{CI}_2, \text{Cro}_2\}$, where \mathcal{X} is the state space, \mathbf{s} is a microstate in \mathcal{X} , $\mathbf{P}(\mathbf{s})$ is the

Algorithm 1 State Enumerator(M, R, B)

Network model: $N \leftarrow \{M, R\}$;
Initial condition: $s^{t=0} \leftarrow \{c_1^0, c_2^0, \dots, c_m^0\}$; Set the value of buffer capacity: $c_{m+1}^0 \leftarrow B$;
Initialize the state space and the set of transitions: $\mathcal{X} \leftarrow \emptyset$; $T \leftarrow \emptyset$;
Stack $ST \leftarrow \emptyset$; Push($ST, s^{t=0}$); $StateGenerated \leftarrow \text{FALSE}$
while $ST \neq \emptyset$ **do**
 $s_j \leftarrow \text{Pop}(ST)$;
 for $k = 1$ to n **do**
 if reaction R_k occurs under condition s_j **then**
 if reaction R_k is a synthetic reaction and generates u_k new molecules **then**
 $c_{m+1} \leftarrow c_{m+1} - u_k$
 if $c_{m+1} \geq 0$ **then**
 Generate state $s(j, R_k)$ that is reached by following reaction R_k from s_j ;
 $StateGenerated \leftarrow \text{TRUE}$
 end if
 else
 if reaction R_k is a degradation reaction and breaks down u_k molecules **then**
 $c_{m+1} \leftarrow c_{m+1} + u_k$
 end if
 Generate state $s(j, R_k)$ that is reached by following reaction R_k from s_j ;
 $StateGenerated \leftarrow \text{TRUE}$
 end if
 if ($StateGenerated = \text{TRUE}$) and ($s(j, R_k) \notin \mathcal{X}$) **then**
 $\mathcal{X} \leftarrow \mathcal{X} \cup s(j, R_k)$;
 Push($ST, s(j, R_k)$);
 $T \leftarrow T \cup t_{s(j, R_k), s_j}$;
 $a_{i,j} \leftarrow \text{Transition Coefficient}(s(j, R_k), s_j, R_k)$
 end if
 end if
 end for
end while
Output \mathcal{X}, T and $A = \{a_{i,j}\}$.

probability of \mathbf{s} in the steady state probability distribution, and \mathbf{s}_m is the copy number of molecular species m in state \mathbf{s} .

S4. Stochastic Model of Epigenetic Switch of Phage Lambda

The architecture of our model of the epigenetic switch for prophage induction is shown in Fig S1. In this model, the O_R region contains the lysogenic promoter P_{RM} for the transcription of the cI gene and the lytic promoter P_R for transcription of the cro gene. Both CI and Cro proteins dimerize and self-regulate through positive feedback loops, at the same time suppresses the expression of the other protein. There are three operator sites in O_R that both CI_2 protein (also called the repressor) and Cro_2 protein bind, but with different affinities. CI_2 maintains the lysogenic state by blocking O_R sites and preventing transcription of lytic genes including cro . As a result, there is continued expression of the CI protein and the suppression of the cro gene. The switch from lysogenic to lytic state depends on reduction of CI_2 levels, which reflects the state of the bacterium.

When DNA is damaged, the protease RecA from the SOS system is activated, which mediates cleavage of CI repressor. When CI is below a certain level, P_R becomes depressed and transcription of lytic gene is activated, starting with cro . The switch to lytic state is then thrown [21, 24]. In the lytic state, Cro fully represses CI expression.

In this study, our interest is to model once lysogeny has been established, how phage lambda maintain lysogeny, and how it transits to lytic state at adverse environmental condition. The process of establishing lysogeny is not modeled explicitly. For clarity, we use the term of lysogenic state and lytic state instead of lysogenic pathway and lytic pathway, which are sometimes used in the literature. The rationale is that lysogeny and lysis are physiological conditions rather than a specific sequence of events, as implied by the term of *pathway*.

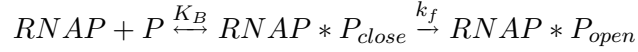
There are a total of 13 molecular species in our model: three empty operator sites ($OR1$, $OR2$ and $OR3$), three operator sites separately bound by CI dimer ($ROR1$, $ROR2$, and $ROR3$), and operator sites separately bound by Cro dimer ($COR1$, $COR2$, and $COR3$), protein monomers (CI and Cro), and protein dimers (CI_2 and Cro_2). Our model is an open system, *i.e.*, there exist synthesis and degradation reactions. A buffer is introduced to limit the state space [6]. The buffer size used in this study, namely, the maximum copy number of net molecules synthesized in the system is 50. This is sufficient to model phage lambda [4, 5]. We do not consider the detailed effects of promoter strengths.

S5. Reactions and Parameters

The 54 biochemical reactions can be classified as synthesis, degradations, dimerizations, binding and dissociation reactions.

Protein synthesis. We follow the approach introduced by Arkin *et al* [2] to model the protein synthesis process. In this approach, the time required for protein synthesis includes that required for the transcription process (transcription initiation and elongation) and the translational process. The rate limiting step in transcription initiation is taken to be the closed- to open-complex isomerization

reaction [12]. Therefore, the rate of the transcription initiation reaction



is taken as $k_f = 6.5 \times 10^4 / M \cdot sec$ (when OR2 is empty) or $9.5 \times 10^5 / M \cdot sec$ (when OR2 is occupied by a repressor) for CI protein and $k_f = 6.7 \times 10^6 / M \cdot sec$ for Cro protein [12, 13, 20]. Transcription elongation rate on average is $= 30$ nt/sec [2, 11, 15, 29], and the elongation time for CI and Cro is calculated based on the length of the coding DNA and is taken as 23.6 and 7.6 sec, respectively. An average of ten copies of proteins are assumed to be produced per transcript for CI and Cro [2, 27]. The translational time for 10 copies of CI and Cro is calculated based on the translational rate of 100 nt/sec [1, 2, 15, 28], and is taken as 7.1 and 2.3 sec for CI and Cro, respectively.

Based on these considerations, transcription and translation of a protein are combined into a single synthesis reaction for simplification. The synthesis reactions and rates are taken from [12, 13] according to [2], and are listed in Table S1. These reactions and parameters are used in both wild type and mutant phage lambda.

Protein degradation. CI and Cro protein degradation is modeled by the proteolysis of the monomeric form, a common degradation mode for multimeric proteins [2, 27]. The values of the rate parameters are taken from [2]. The degradation reactions and reaction rates are listed in Table S1.

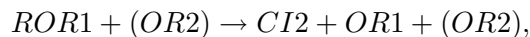
Dimerization reactions. We follow [2] to model the dimerization reactions, in which the parameters were obtained from experimental measurements [2, 27]. The sources of the parameter values as documented in [2, 27] for individual reactions are also listed in Table S1.

Free energy and equilibrium constant of binding/dissociation reactions. We use ΔG to denote the Gibbs free energy of the binding/dissociation reactions. It is related to the equilibrium constant k_{eq} through the relationship:

$$k_{eq} = \exp\left(\frac{-\Delta G}{R \cdot T}\right).$$

It was found experimentally that CI binds to OR1 tightly and to OR3 weakly [16]. Conversely, Cro binds to OR1 and OR2 weakly, but to OR3 tightly. We use ΔG_1 to denote the binding free energy of CI_2 to OR1, ΔG_2 for CI_2 to OR2, and ΔG_3 for CI_2 to OR3, respectively. We use ΔG_{1*} , ΔG_{2*} , and ΔG_{3*} to represent binding free energy of Cro_2 to OR1, OR2, and OR3, respectively. The binding free energies of CI repressor to the operators are listed in Table S3 and are taken from Koblan and Ackers [16], those of Cro are from Darling *et al.* [7].

Free energy change due to cooperativities of CI_2 and Cro_2 bound to neighboring operator sites. Following the approach described in [7, 16], we explicitly incorporate cooperativity between repressor CI dimers binding on adjacent operator sites (Fig S2). That is, CI_2 dimer binding on OR1 promotes binding of another CI_2 on OR2. This is reflected by a modification to the free energy change for the dissociation interaction. Specifically, the reaction



has a free energy change $\Delta G_1 = -12.5$ kcal/mol for Cl_2 dissociating from OR1. When a Cl_2 dimer is already bound to the OR2 site, the dissociation reaction of another Cl_2 dimer from OR1



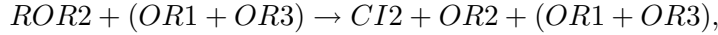
has a larger free energy change and Cl_2 dimers bound on adjacent OR1 and OR2 form a more stable complex, which is modeled by adding a correction term ΔG_{12} due to cooperativity to the original free energy change:

$$\Delta G_{1,coop} = \Delta G_1 + \Delta G_{12}.$$

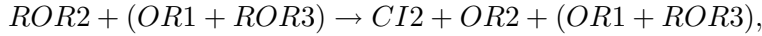
Similarly, we modify the free energy ΔG_2 for Cl_2 dimer dissociating from OR2 if a Cl_2 dimer is already bound to OR1:

$$\Delta G_{2,coop} = \Delta G_2 + \Delta G_{12}.$$

The same approach is used for modeling cooperativity of Cl_2 dissociating from OR2 and OR3. The dissociation reaction



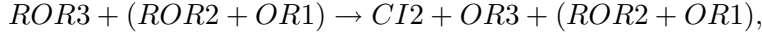
has a free energy change of ΔG_2 . When a Cl_2 dimer is already bound to the OR3 site, the dissociation reaction



has a modification of ΔG_{23} added to ΔG_2 :

$$\Delta G_{2,coop} = \Delta G_2 + \Delta G_{23}.$$

When a Cl_2 dimer is already bound to the OR2 site, the dissociation reaction



also has a modified amount of ΔG_{23} added to ΔG_3 :

$$\Delta G_{3,coop} = \Delta G_3 + \Delta G_{23}.$$

With the same approach, we also explicitly incorporate cooperativity between Cro_2 dimers binding on adjacent operator sites. For the binding cooperativity when Cro_2 dimer binds to OR1 and OR2, and when there is already a Cro_2 dimer bound to OR1 or OR2 site, we add a stabilizing modification term ΔG_{1*2*} to ΔG_{1*} or ΔG_{2*} , respectively. For the binding cooperativity when Cro_2 dimer binds to OR2 and OR3, and when there is already a Cro_2 dimer bound to either of these two sites, we add a stabilizing modification term ΔG_{2*3*} to ΔG_{2*} and ΔG_{3*} accordingly.

In addition, we introduce a cooperativity term ΔG_{1*2*3*} for Cro_2 dimer dissociating from OR1 when both OR2 and OR3 are occupied, and for Cro_2 dissociating from OR3 when both OR1 and OR2 are occupied. In this case, the final binding free energy is modeled as:

$$\Delta G_{1*,coop} = \Delta G_{1*} - \Delta G_{2*3*} + \Delta G_{1*2*3*}$$

and

$$\Delta G_{3*,coop} = \Delta G_{3*} - \Delta G_{1*2*} + \Delta G_{1*2*3*}$$

respectively.

The free energy changes due to these cooperativities for CI are taken from Koblan and Ackers [16], those of Cro are from Darling *et al.* [7], and are listed in Table S3.

Other cooperativity effects. Our model implicitly models the cooperative effect of looping between OR and OL. The cooperativity due to the looping effect stabilizes CI₂ binding to OR2, leading to increased CI synthesis [20]. This is reflected by about 10 fold increase in CI synthesis rate when OR2 is CI₂-bound as shown in Table S3.

In addition, the suppression of the P_{RM} of CI bound to OR3 is also included in our model, which would not be possible without the looping effects between OL and OR.

Association rates of protein binding to operators. We assume CI₂ and Cro₂ proteins have equal access to the operators on DNA. The association rate constant $k_a = 2.57 \times 10^7 / M \cdot sec$ is derived from experimentally measured protein diffusion coefficient $10^{-7} cm^2/s$ [8], which is within the *in vitro* measured range ($10^6 - 10^8 / M \cdot sec$) of CI binding to OR1, OR2, and OR3 [22]. In order to calculate the mesoscopic rate constant for binding reactions involving two reactants, we need to divide k_a by $A \cdot V$, in which $A = 6.023 \times 10^{23}$ is the Avogadro's number and $V = 2 \times 10^{-15} l$ is roughly the volume of *E. coli* cell [17]. We use the resulting rate constant $K_{b_DimerDNA} = k_a / A \cdot V = 0.021 / sec$,

Dissociation rates of CI₂ and Cro₂ from operator sites.

Wild type phage lambda. We follow the model in reference [2], and assume the binding of CI₂ and Cro₂ to the operator sites have the same association rates but different dissociation rates. The dissociation rate k_d is calculated from the equilibrium constant k_{eq} :

$$k_d = k_a / k_{eq},$$

where k_a is the association rate, and $k_{eq} = \exp(\frac{-\Delta G}{R \cdot T})$, ΔG is the Gibbs free energy of the binding reactions, R is the universal gas constant, and $T = 310.15$ Kelvin (*i.e.*, 37 Celsius) is the absolute temperature at which the experiments were performed. The resulting values of dissociation rates of CI₂ and Cro₂ from OR1, OR2, and OR3 calculated from Gibbs free energies are listed in Table S2.

Mutant 1-2-1. Following Little *et al*, we assume that mutations do not alter the properties of the P_{RM} and P_R promoters but affect only binding interactions of Cro₂ and CI₂ to OR [21]. In mutant 1-2-1, an OR1 operator replaces the original OR3. Based on parameters reported in [7, 16], we have now $\Delta G_3 = \Delta G_1 = -12.5$ kcal/mol, and $\Delta G_{3*} = \Delta G_{1*} = -12.0$ kcal/mol. In addition, we have $\Delta G_{23} = \Delta G_{12} = -2.7$ kcal/mol, and $\Delta G_{2*3*} = \Delta G_{1*2*} = -1.0$ kcal/mol. The dissociation rates of mutant 1-2-1 are then calculated using the appropriate modified ΔG values (Table S3).

Mutant 1-2-3. In this mutant, operators OR1 and OR3 exchange places. Based on parameters reported in [7, 16], we have now $\Delta G_1 = -9.5$ kcal/mol, $\Delta G_3 = -12.5$ kcal/mol, $\Delta G_{1*} = -13.4$ kcal/mol, and $\Delta G_{3*} = -12.0$ kcal/mol. In addition, we have $\Delta G_{12} = -2.9$ kcal/mol, $\Delta G_{23} = -2.7$ kcal/mol, $\Delta G_{1*2*} = -0.6$ kcal/mol, and $\Delta G_{2*3*} = -1.0$ kcal/mol. The dissociation rates of mutant 1-2-3 are then calculated accordingly (Table S3).

Mutant 3-2-3. In this mutant, operator OR3 replaces the original OR1. Based on parameters reported in [7, 16], we have now $\Delta G_1 = \Delta G_3 = -9.5$ kcal/mol, and $\Delta G_{1*} = \Delta G_{3*} = -13.4$ kcal/mol. In addition, we have $\Delta G_{12} = \Delta G_{23} = -2.9$ kcal/mol, and $\Delta G_{1*2*} = \Delta G_{2*3*} = -0.6$ kcal/mol. The dissociation rates of mutant 3-2-3 are then calculated accordingly (Table S3).

Mutant 3'-2-3'. This mutant is similar to mutant 3-2-3, with the difference of one nucleotide in OR3 replaced by one from OR1 [21]. Based on experimental data reported in [7, 21], we have the modification

of $\Delta\Delta G_3 = -0.8$ kcal/mol to the binding free energy ΔG_3 of CI_2 to OR3, and $\Delta\Delta G_{3^*} = 1.3$ kcal/mol to the binding free energy ΔG_{3^*} of Cro_2 to OR3 (Fig. 4 from [21]). From these considerations, we have $\Delta G_1 = \Delta G_3 = \Delta G_1 + \Delta\Delta G_3 = -13.3$ kcal/mol for CI_2 binding, and $\Delta G_{1^*} = \Delta G_{3^*} = \Delta G_{1^*} + \Delta\Delta G_{3^*} = -10.7$ kcal/mol for Cro_2 dimer binding.

Additionally, since we replaced the original OR1 with OR3', we have $\Delta G_{12} = \Delta G_{23} = -2.9$ kcal/mol, and $\Delta G_{1^*2^*} = \Delta G_{2^*3^*} = -0.6$ kcal/mol. As the cooperativities of CI_2 and Cro_2 between OR2 and OR3' have not been measured, we use the values of cooperativity between OR2 and OR3 instead. The dissociate rates of mutant 3'-2-3' are calculated accordingly (Table S3).

Free proteins and DNA bound proteins. Our goal is to study the stochastic effects of the phage lambda network, which are most prominent when the copy numbers of molecules are small. Here we make the assumption that only the free concentration of the regulatory proteins contributes to specific binding. The fluctuation of the number of DNA-bound CI dimer is not modeled explicitly. The total number of CI molecules is often thought to be in the range of 100 to 500 [3]. However, there exists significant amount of nonspecific binding of CI and Cro proteins to DNA at regions other than the operators, which may account for about 86% of the total of about 250 of CI monomers in lysogen. Since there is about only 10 copies of free CI dimers in a lysogenic cell [4, 5], we set the total maximum number of free CI monomers to be 50 copies. This choice of the upper limit offers the additional advantages in facilitating large scale computational investigations necessary when studying systematically the behavior of the phage lambda regulatory network at different conditions.

Probability Landscape of Wild Type and Mutant Phage Lambda. The probability landscape of wild type projected in the space of CI_2 and Cro_2 at five different CI degradation rates k_d (lysogeny, start of transition, transition, end of transition, and lysis) are plotted in Fig S3. Probability landscape of 4 mutant phage lambda at the same degradation rates are also plotted.

Effects of Cooperativity on Probability Landscape of Wild Type and Mutant Phage Lambda The probability landscapes of wild type phage lambda with all cooperativities intact, with all cooperativities removed, with only cooperativity between CI_2 binding to O_R1 and O_R2 restored, with all but that between CI_2 binding to O_R1 and O_R2 restored at different K_d are shown in in Fig S4. The probability landscapes of mutant 1-2-1 are shown in Fig S5.

S6. Comparisons to Other Methods

In this section, we compare results from our method with results from the stochastic simulation algorithm [9], a stochastic differential equation (SDE) model, and a deterministic ODE model.

Stochastic Simulation Algorithm. Stochastic simulation algorithm [9] is a widely used method for simulating biochemical reaction systems. However, it is inefficient in simulating rare events, such as the transition between lysogenic and lytic states in phage lambda. To study how this transition is affected by different parameters such as different UV irradiation, it is important to characterize the probability distribution of the switching network at the transition state.

We illustrate here how the stochastic simulation algorithm (SSA) and our direct chemical master equation (dCME) method differ in computing the steady state probability distribution of the phage lambda in transition phase. We use exactly the same model and parameters for both methods. With the wild-type phage lambda model, we set the CI degradation rate $k_d = 0.0020/s$ so the decision network is in the transition state. We start SSA simulation from three different initial conditions: (1) all protein monomer and dimer are initially zero concentration; (2) 10 copies of CI monomers and dimers each, and zero copies of Cro monomer and dimer; (3) 10 copies of Cro monomers and dimers each, but zero copies of CI monomer and dimer. Because of the Markovian properties of the system, all simulations should give the same steady state distribution. We run calculation and simulations in single thread mode on the same machine with 2GHz AMD Quad Core CPU. We use the STOCHKIT package for SSA simulations [19].

The exact solution of the chemical master equation using dCME method was obtained in < 8 hours. The steady state probability distribution is shown in Fig 2b in the main text. Fig S6 shows the probability distributions we obtained from stochastic simulation after 1, 12, 24, 36, and 48 hours of calculation, respectively. It can be seen that after 48 hour, the simulation had not yet converged, as the probability landscape distributions are different for simulations run at the three different initial conditions. In fact, some of these simulations would erroneously lead to the conclusion that the steady state is still predominantly lysogenic if certain initial conditions are chosen. We calculate the residual error between the probability landscape computed in 48-hour of stochastic simulations and that computed from dCME in < 8 hours of calculation (last row of Fig. S6). Here residual errors are obtained by subtracting the probability landscapes of stochastic simulation at 48 hours (Fig. S6) from the directly solved landscape of chemical master equation (Fig. 2b). After 48 hours of simulation, the differences between these probability landscapes are still large. This example indicates that the stochastic simulation algorithm in this case is neither accurate nor efficient for studying rare events.

We have also compared probability landscapes computed from dCME and from SSA for the system in other regions: in the lysogenic region ($k_d = 0.0007/s$), at the beginning of the transition region ($k_d = 0.0018/s$), at the end of the transition region ($k_d = 0.0022/s$), and in the lytic region ($k_d = 0.0036/s$), each with three different initial conditions. Fig S7 summarizes the residual errors in landscape from SSA simulations and Fig S8 shows the errors in estimated mean copies of CI_2 and Cro_2 after 8 hours of simulation, Fig S9 and Fig S10 show errors after 48 hours of simulation. Our results show that in all cases, the probability landscape obtained from SSA depend on initial condition. We find that error in landscape remains large when the system start to enter the lytic region ($k_d = 0.0022/s$), and the expected copy number of CI_2 can be over-estimated by 300% and 150% after 8 hours and 48 hours of computation, respectively. In addition, the small amount of Cro_2 calculated in the lysogenic condition can be off by 3-order of magnitude.

Deterministic ODE Model. We built an ordinary differential equation (ODE) model following the deterministic formulation of Santillán and Mackey [25]. To facilitate a direct comparison, the O_L operators are omitted, and the same parameter values as in the dCME model are used. Correspondingly, the transcription and translation of CI and Cro are model here as two synthesis reactions, one for each protein. The synthesis rate of CI monomer is calculated as the product of the probability of promoter P_{RM} being occupied by RNA polymerase ($f_{RM}^c([CI_2], [Cro_2])$ when CI_2 is bound on O_{R2} , $f_{RM}([CI_2], [Cro_2])$ when O_{R2} is unoccupied by CI_2), times the rate constant of CI synthesis ($k_{s,CI}^c$ when CI_2 is bound on O_{R2} , and $k_{s,CI}$ when O_{R2} is unoccupied by CI_2). The synthesis rate of Cro monomer is calculated as the the product of probability of promoter P_R being occupied by the RNA

polymerase ($f_R([CI_2], [Cro_2])$), times the rate constant of synthesis $k_{s,Cro}$.

The same model of thermodynamics of interactions between protein dimers and O_R operator sites of Shea and Ackers [27] is used to calculate the probabilities $f_{RM}^c([CI_2], [Cro_2])$, $f_{RM}([CI_2], [Cro_2])$, and $f_R([CI_2], [Cro_2])$. The rate constants of CI and Cro synthesis take the same values as in the dCME model (Table S1).

Following the formulation of Santillán and Mackey [25], we use the quasi-steady state assumption to approximately calculate the amount of CI and Cro dimers from monomers, although dimer association and dissociation reactions of CI and Cro are explicitly modeled in the dCME study. The equilibrium CI and Cro dissociation constants K_D^{CI} and K_D^{Cro} necessary for this approximation are calculated from the association and dissociation rates of the dimerization reactions listed in Table S1. We have: $K_D^{CI} = 0.5s^{-1}/0.05nM^{-1}s^{-1} = 10nM = 0.01\mu M$, and $K_D^{Cro} = 0.5s^{-1}/0.0307nM^{-1}s^{-1} \approx 16.3nM = 0.0163\mu M$. Our ODE model can be summarized as:

$$\frac{d[CI]}{dt} = k_{s,CI}^c f_{RM}^c([CI_2], [Cro_2]) + k_{s,CI} f_{RM}([CI_2], [Cro_2]) - k_{d,CI}[CI], \quad (6)$$

$$\frac{d[Cro]}{dt} = k_{s,Cro} f_R([CI_2], [Cro_2]) - k_{d,Cro}[Cro], \quad (7)$$

and

$$[CI_2] = \frac{1}{2}[CI] - \frac{K_D^{CI}}{8} \left[\sqrt{1 + 8 \frac{[CI]}{K_D^{CI}}} - 1 \right], \quad (8)$$

$$[Cro_2] = \frac{1}{2}[Cro] - \frac{K_D^{Cro}}{8} \left[\sqrt{1 + 8 \frac{[Cro]}{K_D^{Cro}}} - 1 \right] \quad (9)$$

where $k_{s,CI}^c = 0.066/s$ is the synthesis rate of CI monomer with a CI dimer bound on O_R2 , $k_{s,CI} = 0.0069/s$ is the CI synthesis rate without CI dimer bound on O_R2 , and $k_{s,Cro} = 0.0929/s$ is the synthesis rate of Cro. $k_{d,CI}$ and $k_{d,Cro}$ are degradation rates of CI and Cro. $k_{d,Cro}$ takes a fixed value of 0.0025/s, and the value of $k_{d,CI}$ is changed systematically from 0.0001/s to 0.0036/s.

The bifurcation curves of the steady state of the ODE model for the wild-type phage lambda and the Little's mutants are shown in Fig. S11. Red lines represent the concentrations of CI_2 at different CI degradation rate, and blue lines represent that of Cro_2 . Comparison with Fig. 3 and 4 in the main text shows that there are at least three major qualitative differences between these two approaches. First, results from the ODE model (Fig. S11a) lacks the ability in maintaining a relatively stable amount of CI dimer in wild-type phage lambda when CI degradation rate increases, unlike results from the chemical master equation model (Fig. 3a, solid line in the main text). Rather, the amount of CI dimer rapidly decreases when CI degradation rate increases. Second, the overall behavior of wild type and mutant 1-2-1 phage lambda do not show appreciable differences other than the transition point (Fig. S11a and b), whereas they are significantly different in results from the chemical master equation model (Fig 3a,c solid lines in the main text). Third, results from the ODE model show that the transition point from lysogenic to lytic state occurs at a later stage in mutants 3'-2-3' and 1-2-1 than in wild-type (Fig. S11a, b and c), which would suggest that that mutant 1-2-1 and 3'-2-3' would be more stable against the UV irradiation than the wild-type, whereas our results (Fig. 3a, solid line, Fig. 4a and b) show that these mutants have a hair trigger and lack the stability against UV irradiation, in agreement with experimental observations [21].

This comparison is important, as ODE model provides the “skeleton” of all stochastic models (both dCME and SDE models), and a full grasp of the corresponding deterministic ODE will help to gain a thorough understanding of the dCME model.

Model of Stochastic Differential Equation. We also compare our results with that of stochastic differential equation (SDE). Following the approach described in reference [10], we derive the SDE model by extending the ODE model discussed above. The model takes the following form:

$$d[\text{CI}] = S_{\text{CI}}dt - D_{\text{CI}}dt + \sqrt{S_{\text{CI}}dt} \cdot \mathcal{N}_1(0, 1) - \sqrt{D_{\text{CI}}dt} \cdot \mathcal{N}_2(0, 1), \quad (10)$$

$$d[\text{Cro}] = S_{\text{Cro}}dt - D_{\text{Cro}}dt + \sqrt{S_{\text{Cro}}dt} \cdot \mathcal{N}_3(0, 1) - \sqrt{D_{\text{Cro}}dt} \cdot \mathcal{N}_4(0, 1), \quad (11)$$

where

$$S_{\text{CI}} = k_{s,\text{CI}}^c f_{RM}^c([\text{CI}_2], [\text{Cro}_2]) + k_{s,\text{CI}} f_{RM}([\text{CI}_2], [\text{Cro}_2]), \quad (12)$$

$$D_{\text{CI}} = k_{d,\text{CI}}[\text{CI}], \quad (13)$$

$$S_{\text{Cro}} = k_{s,\text{Cro}} f_R([\text{CI}_2], [\text{Cro}_2]), \quad (14)$$

$$D_{\text{Cro}} = k_{d,\text{Cro}}[\text{Cro}] \quad (15)$$

and $\mathcal{N}_1(0, 1), \mathcal{N}_2(0, 1), \mathcal{N}_3(0, 1)$, and $\mathcal{N}_4(0, 1)$ are independent Gaussian noises with mean of 0 and variance of 1.

We set $k_{d,\text{CI}} = 0.0020/s$ so the system is in the transition phase, and monitor the rate of convergence of the SDE simulations when starting with different initial conditions. The initial conditions are: (1) both concentrations of CI and Cro monomers are $0 \mu M$: $[\text{CI}]_0 = [\text{Cro}]_0 = 0 \mu M$; (2) $[\text{CI}]_0 = 0.1 \mu M, [\text{Cro}]_0 = 0 \mu M$; and (3) $[\text{CI}]_0 = 0 \mu M, [\text{Cro}]_0 = 0.1 \mu M$. Here only concentrations of monomers are specified, dimer concentrations are calculated as in the above ODE model.

Our dCME model results show that the system is in the transition phase when $k_{d,\text{CI}} = 0.0020/s$, while SDE model shows the system is completely in lytic state. That is, the SDE model has not converged after 48 hours, 6 times of the 8 hours required by the dCME model (Fig. S12). This suggests that it is challenging to produce accurate results using SDE model for the phage lambda system. Further study is required to obtain a comprehensive understanding of the behavior and limitations of SDE models.

S7. Additional information on comparison with a previous theoretical study

Zhu *et al.* modeled the phage lambda switching network through a potential surface reconstructed from a stochastic differential equation model [30]. They found that the wild-type phage lambda was not significantly affected when the cooperative binding of CI dimers is reduced by half. Our results show that the titration curve of the CI concentration against increases in CI degradation rate depends significantly on the cooperative binding free energy between CI dimers on O_R1 and O_R2 (ΔG_{12}). Fig. S13 shows the titration curves at cooperative binding free energy (ΔG_{12}) multiplied by a factor of 0.0, 0.5, 0.8, and 1.2, respectively. When the binding free energy is reduced by a factor of 0.5, the switching threshold at about 50% induction is decreased from $k_d = 0.0020/s$ to $k_d = 0.0007/s$. If the cooperative binding free energy is increased by a factor 1.2, the switching threshold is raised to $k_d = 0.0028/s$. Therefore, we find that the resistance of wild type phage to the UV irradiation

is strongly affected by the cooperative binding: the larger the cooperativity the stronger resistance phage lambda is to the UV irradiation. In contrast, Zhu *et al*'s calculation suggested that there is little change in stability for wild type phage lambda [30].

References

- [1] S. Adhya and M. Gottesman, *Promoter occlusion: transcription through a promoter may inhibit its activity*, Cell **29** (1982), no. 3, 939–944.
- [2] A. Arkin, J. Ross, and H. H. McAdams, *Stochastic kinetic analysis of developmental pathway bifurcation in phage lambda-infected Escherichia coli cells.*, Genetics **149**(4) (1998), 1633–1648.
- [3] Erik Aurell, Stanley Brown, Johan Johanson, and Kim Sneppen, *Stability puzzles in phage λ* , Physical Review E **65** (2002), no. 5, 051914.
- [4] A. Bakk and R. Metzler, *In vivo non-specific binding of lambda CI and Cro repressors is significant*, FEBS Letters **563** (2004), no. 1-3, 66–68.
- [5] A. Bakk and R. Metzler, *Nonspecific binding of the OR repressors CI and Cro of bacteriophage lambda*, Journal of theoretical biology **231** (2004), no. 4, 525–533.
- [6] Youfang Cao and Jie Liang, *Optimal enumeration of state space of finitely buffered stochastic molecular networks and exact computation of steady state landscape probability*, BMC Systems Biology **2** (2008), 30.
- [7] Paul J. Darling, Jo M. Holt, and Gary K. Ackers, *Coupled energetics of λ cro repressor self-assembly and site-specific DNA operator binding II: Cooperative interactions of cro dimers*, Journal of Molecular Biology **302** (2000), no. 3, 625–638.
- [8] Michael B. Elowitz, Michael G. Surette, Pierre-Etienne Wolf, Jeffry B. Stock, and Stanislas Leibler, *Protein Mobility in the Cytoplasm of Escherichia coli*, J. Bacteriol. **181** (1999), no. 1, 197–203.
- [9] D. T. Gillespie, *Exact stochastic simulation of coupled chemical reactions*, Journal of Physical Chemistry **81** (1977), 2340–2361.
- [10] D.T. Gillespie, *The chemical Langevin equation*, The Journal of Chemical Physics **113** (2000), 297.
- [11] SL Gotta, OL Miller Jr, and SL French, *rRNA transcription rate in Escherichia coli.*, Journal of bacteriology **173** (1991), no. 20, 6647.
- [12] D. Hawley and W. McClure, *In vitro comparison of initiation properties of bacteriophage lambda wild-type pr and x3 mutant promoters.*, Proc Natl Acad Sci U S A **77**(11) (1980), 6381–6385.
- [13] D. Hawley and W. McClure, *Mechanism of activation of transcription initiation from the lambda prm promoter.*, J Mol Biol **157**(3) (1982), 493–525.
- [14] S. Kachalo, H. Lu, and J. Liang, *Protein folding dynamics via quantification of kinematic energy landscape.*, Phys Rev Lett **96**(5) (2006), 058106.

- [15] D. Kennell and H. Riezman, *Transcription and translation initiation frequencies of the Escherichia coli lac operon*, Journal of Molecular Biology **114** (1977), no. 1, 1–21.
- [16] Kenneth S. Koblan and Gary K. Ackers, *Site-specific enthalpic regulation of DNA transcription at bacteriophage λ OR*, Biochemistry **31** (1992), 57–65.
- [17] Céline Kuttler and Joachim Niehren, *Gene Regulation in the Pi Calculus: Simulating Cooperativity at the Lambda Switch*, Transactions on Computational Systems Biology VII **4230** (2006), 24–55.
- [18] R. Lehoucq, D. Sorensen, and C. Yang, *Arpack users’ guide: Solution of large scale eigenvalue problems with implicitly restarted arnoldi methods*, SIAM, Philadelphia, 1998.
- [19] H. Li, Y. Cao, L.R. Petzold, and D.T. Gillespie, *Algorithms and software for stochastic simulation of biochemical reacting systems*, Biotechnology progress **24** (2008), no. 1, 56.
- [20] M. Li, W. McClure, and M. Susskind, *Changing the mechanism of transcriptional activation by phage lambda repressor.*, Proc Natl Acad Sci U S A **94**(8) (1997), 3691–3696.
- [21] John W. Little, Donald P. Shepley, and David W. Wert, *Robustness of a gene regulatory circuit*, The EMBO Journal **18** (1999), no. 15, 4299–4307.
- [22] E. Merabet and G.K. Ackers, *Calorimetric analysis of lambda cI repressor binding to DNA operator sites*, Biochemistry **34** (1995), 8554–8563.
- [23] Brian Munsky and Mustafa Khammash, *The finite state projection algorithm for the solution of the chemical master equation*, The Journal of Chemical Physics **124** (2006), no. 4, 044104.
- [24] Mark Ptashne, *A genetic switch: Phage lambda revisited.*, Cold Spring Harbor Laboratory Press; 3 edition, 2004.
- [25] Moises Santillán and Michael C. Mackey, *Why the Lysogenic State of Phage lambda Is So Stable: A Mathematical Modeling Approach*, Biophys. J. **86** (2004), no. 1, 75–84.
- [26] D. Schultz, J. N. Onuchic, and P. G. Wolynes, *Understanding stochastic simulations of the smallest genetic networks.*, J Chem Phys **126**(24) (2007), 245102.
- [27] Madeline A. Shea and Gary K. Ackers, *The OR control system of bacteriophage lambda a physical-chemical model for gene regulation*, Journal Molecular Biology **181** (1985), no. 2, 211–230.
- [28] M.A. Sørensen and S. Pedersen, *Absolute in vivo translation rates of individual codons in Escherichia coli: The two glutamic acid codons GAA and GAG are translated with a threefold difference in rate*, Journal of molecular biology **222** (1991), no. 2, 265–280.
- [29] U. Vogel and KF Jensen, *The RNA chain elongation rate in Escherichia coli depends on the growth rate.*, Journal of bacteriology **176** (1994), no. 10, 2807.
- [30] X.-M. Zhu, L. Yin, L. Hood, and P. Ao, *Robustness, stability and efficiency of phage lambda genetic switch: dynamical structure analysis*, Journal of Bioinformatics and Computational Biology **2** (2004), 785–817.

Table S1: Reactions and associated parameters. These reactions and parameter values are common for wild type and all mutants. Here $COR2$ denotes Cro_2 dimer-bound OR2, $ROR2$ denotes CI_2 dimer-bound OR2. Note that molecular species enclosed in parenthesis are those whose presence is required for the specific reactions to occur, but their copy numbers do not influence the transition rates between microstates.

Reactions	Rates(k)
Synthesis reactions [2, 12, 13, 20]	
$\emptyset + (OR3 + OR2) \rightarrow CI + (OR3 + OR2)$	0.0069/s
$\emptyset + (OR3 + COR2) \rightarrow CI + (OR3 + COR2)$	0.0069/s
$\emptyset + (OR3 + ROR2) \rightarrow CI + (OR3 + ROR2)$	0.066/s
$\emptyset + (OR1 + OR2) \rightarrow Cro + (OR1 + OR2)$	0.0929/s
Degradation reactions [2, 27]	
$CI \rightarrow \emptyset$	0.0007/s
$Cro \rightarrow \emptyset$	0.0025/s
Dimerising reactions [2, 27]	
$2 \times CI \rightarrow CI_2$	$0.05/nM \cdot s$
$2 \times Cro \rightarrow Cro_2$	$0.0307/nM \cdot s$
$CI_2 \rightarrow 2 \times CI$	0.5/s
$Cro_2 \rightarrow 2 \times Cro$	0.5/s
Association rate of binding reactions [17]	
$CI_2 + OR1 \rightarrow ROR1$	0.021/s
$CI_2 + OR2 \rightarrow ROR2$	0.021/s
$CI_2 + OR3 \rightarrow ROR3$	0.021/s
$Cro_2 + OR1 \rightarrow COR1$	0.021/s
$Cro_2 + OR2 \rightarrow COR2$	0.021/s
$Cro_2 + OR3 \rightarrow COR3$	0.021/s

Table S2: Reactions and their parameters (continued). This table lists dissociation reactions and their rates in wild type phage lambda. Rates of dissociation for other mutants of phage lambda can be calculated by substituting corresponding free energies with those values listed in Table S3.

Reactions	ΔG_s (kcal/mol)	Rates(s^{-1})
Dissociation reactions - CI_2 dissociation from OR1		
$ROR1 + (OR2) \rightarrow CI2 + OR1 + (OR2)$	$\Delta G_1 = -12.5$	0.03998/s
$ROR1 + (ROR2 + OR3) \rightarrow CI2 + OR1 + (ROR2 + OR3)$	$\Delta G_1 + \Delta G_{12} = -15.2$	0.0005/s
$ROR1 + (ROR2 + ROR3) \rightarrow CI2 + OR1 + (ROR2 + ROR3)$	$\Delta G_1 + \Delta G_{12} - \Delta G_{23} = -12.3$	0.05531/s
$ROR1 + (ROR2 + COR3) \rightarrow CI2 + OR1 + (ROR2 + COR3)$	$\Delta G_1 + \Delta G_{12} = -15.2$	0.0005/s
$ROR1 + (COR2) \rightarrow CI2 + OR1 + (COR2)$	$\Delta G_1 = -12.5$	0.03998/s
Dissociation reactions - CI_2 dissociation from OR2		
$ROR2 + (OR1 + OR3) \rightarrow CI2 + OR2 + (OR1 + OR3)$	$\Delta G_2 = -10.5$	1.026/s
$ROR2 + (ROR1 + OR3) \rightarrow CI2 + OR2 + (ROR1 + OR3)$	$\Delta G_2 + \Delta G_{12} = -13.2$	0.01284/s
$ROR2 + (OR1 + ROR3) \rightarrow CI2 + OR2 + (OR1 + ROR3)$	$\Delta G_2 + \Delta G_{23} = -13.4$	0.00928/s
$ROR2 + (ROR1 + ROR3) \rightarrow CI2 + OR2 + (ROR1 + ROR3)$	$\Delta G_2 + \Delta G_{12} = -13.2$	0.01284/s
$ROR2 + (COR1 + OR3) \rightarrow CI2 + OR2 + (COR1 + OR3)$	$\Delta G_2 = -10.5$	1.026/s
$ROR2 + (OR1 + COR3) \rightarrow CI2 + OR2 + (OR1 + COR3)$	$\Delta G_2 = -10.5$	1.026/s
$ROR2 + (COR1 + COR3) \rightarrow CI2 + OR2 + (COR1 + COR3)$	$\Delta G_2 = -10.5$	1.026/s
$ROR2 + (ROR1 + COR3) \rightarrow CI2 + OR2 + (ROR1 + COR3)$	$\Delta G_2 + \Delta G_{12} = -13.2$	0.01284/s
$ROR2 + (COR1 + ROR3) \rightarrow CI2 + OR2 + (COR1 + ROR3)$	$\Delta G_2 + \Delta G_{23} = -13.4$	0.00928/s
Dissociation reactions - CI_2 dissociation from OR3		
$ROR3 + (OR2) \rightarrow CI2 + OR3 + (OR2)$	$\Delta G_3 = -9.5$	5.19753/s
$ROR3 + (ROR2 + OR1) \rightarrow CI2 + OR3 + (ROR2 + OR1)$	$\Delta G_3 + \Delta G_{23} = -12.4$	0.04702/s
$ROR3 + (ROR2 + ROR1) \rightarrow CI2 + OR3 + (ROR2 + ROR1)$	$\Delta G_3 = -9.5$	5.19753/s
$ROR3 + (ROR2 + COR1) \rightarrow CI2 + OR3 + (ROR2 + COR1)$	$\Delta G_3 + \Delta G_{23} = -12.4$	0.04702/s
$ROR3 + (COR2) \rightarrow CI2 + OR3 + (COR2)$	$\Delta G_3 = -9.5$	5.19753/s
Dissociation reactions - Cro_2 dissociation from OR1		
$COR1 + (OR2) \rightarrow Cro2 + OR1 + (OR2)$	$\Delta G_{1*} = -12.0$	0.08999/s
$COR1 + (ROR2) \rightarrow Cro2 + OR1 + (ROR2)$	$\Delta G_{1*} = -12.0$	0.08999/s
$COR1 + (COR2 + OR3) \rightarrow Cro2 + OR1 + (COR2 + OR3)$	$\Delta G_{1*} + \Delta G_{1*2*} = -13.0$	0.01776/s
$COR1 + (COR2 + ROR3) \rightarrow Cro2 + OR1 + (COR2 + ROR3)$	$\Delta G_{1*} + \Delta G_{1*2*} = -13.0$	0.01776/s
$COR1 + (COR2 + COR3) \rightarrow Cro2 + OR1 + (COR2 + COR3)$	$\Delta G_{1*} + \Delta G_{1*2*3*} - \Delta G_{2*3*} = -12.3$	0.05531/s
Dissociation reactions - Cro_2 dissociation from OR2		
$COR2 + (OR1 + OR3) \rightarrow Cro2 + OR2 + (OR1 + OR3)$	$\Delta G_{2*} = -10.8$	0.6306/s
$COR2 + (ROR1 + OR3) \rightarrow Cro2 + OR2 + (ROR1 + OR3)$	$\Delta G_{2*} = -10.8$	0.6306/s
$COR2 + (OR1 + ROR3) \rightarrow Cro2 + OR2 + (OR1 + ROR3)$	$\Delta G_{2*} = -10.8$	0.6306/s
$COR2 + (ROR1 + ROR3) \rightarrow Cro2 + OR2 + (ROR1 + ROR3)$	$\Delta G_{2*} = -10.8$	0.6306/s
$COR2 + (COR1 + OR3) \rightarrow Cro2 + OR2 + (COR1 + OR3)$	$\Delta G_{2*} + \Delta G_{1*2*} = -11.8$	0.12448/s
$COR2 + (OR1 + COR3) \rightarrow Cro2 + OR2 + (OR1 + COR3)$	$\Delta G_{2*} + \Delta G_{2*3*} = -11.4$	0.23822/s
$COR2 + (COR1 + COR3) \rightarrow Cro2 + OR2 + (COR1 + COR3)$	$\Delta G_{2*} + \Delta G_{1*2*3*} = -11.7$	0.14641/s
$COR2 + (ROR1 + COR3) \rightarrow Cro2 + OR2 + (ROR1 + COR3)$	$\Delta G_{2*} + \Delta G_{2*3*} = -11.4$	0.23822/s
$COR2 + (COR1 + ROR3) \rightarrow Cro2 + OR2 + (COR1 + ROR3)$	$\Delta G_{2*} + \Delta G_{1*2*} = -11.8$	0.12448/s
Dissociation reactions - Cro_2 dissociation from OR3		
$COR3 + (OR2) \rightarrow Cro2 + OR3 + (OR2)$	$\Delta G_{3*} = -13.4$	0.00928/s
$COR3 + (ROR2) \rightarrow Cro2 + OR3 + (ROR2)$	$\Delta G_{3*} = -13.4$	0.00928/s
$COR3 + (COR2 + OR1) \rightarrow Cro2 + OR3 + (COR2 + OR1)$	$\Delta G_{3*} + \Delta G_{2*3*} = -14.0$	0.00351/s
$COR3 + (COR2 + ROR1) \rightarrow Cro2 + OR3 + (COR2 + ROR1)$	$\Delta G_{3*} + \Delta G_{2*3*} = -14.0$	0.00351/s
$COR3 + (COR2 + COR1) \rightarrow Cro2 + OR3 + (COR2 + COR1)$	$\Delta G_{3*} + \Delta G_{1*2*3*} - \Delta G_{1*2*} = -13.3$	0.01092/s

Table S3: Free energies of wild type phage and mutants from [7, 16]. The subscripts of ΔG , 1, 2, and 3 stand for binding energies of Cl_2 to OR1, OR2 and OR3, respectively. Accordingly, 1*, 2* and 3* are for the binding Cro_2 to OR1, OR2 and OR3, respectively. The subscripts of ΔG , 12 and 23 stand for cooperatively binding energies of Cl_2 among OR1-OR2 and OR2-OR3, respectively. Accordingly, 1*2*, 2*3*, and 1*2*3* stand for cooperatively binding energies of Cro_2 among OR1-OR2, OR2-OR3, and OR1-OR2-OR3, respectively.

$\Delta G(\text{kcal/mol})$	WT	1-2-1	3-2-3	1-2-3	3'-2-3'
ΔG_1	-12.5	-12.5	-9.5	-9.5	-13.3
ΔG_2	-10.5	-10.5	-10.5	-10.5	-10.5
ΔG_3	-9.5	-12.5	-9.5	-12.5	-13.3
ΔG_{1*}	-12.0	-12.0	-13.4	-13.4	-10.7
ΔG_{2*}	-10.8	-10.8	-10.8	-10.8	-10.8
ΔG_{3*}	-13.4	-12.0	-13.4	-12.0	-10.7
ΔG_{12}	-2.7	-2.7	-2.9	-2.9	-2.9
ΔG_{23}	-2.9	-2.7	-2.9	-2.7	-2.9
ΔG_{1*2*}	-1.0	-1.0	-0.6	-0.6	-0.6
ΔG_{2*3*}	-0.6	-1.0	-0.6	-1.0	-0.6
ΔG_{1*2*3*}	-0.9	-0.9	-0.9	-0.9	-0.9

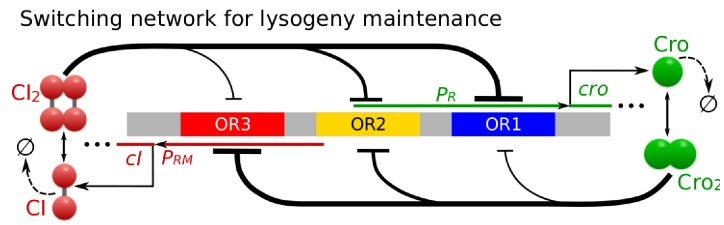


Figure S1: Model of the epigenetic circuit for lysogeny maintenance.

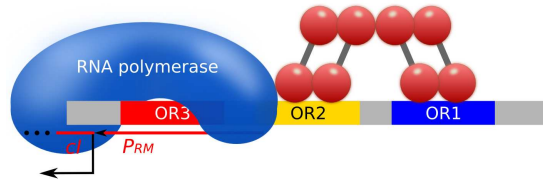


Figure S2: An example of cooperative binding in our model. When either of O_{R1} or O_{R2} site is occupied by Cl_2 , the next Cl_2 will bind to the remaining empty site with enhanced affinity.

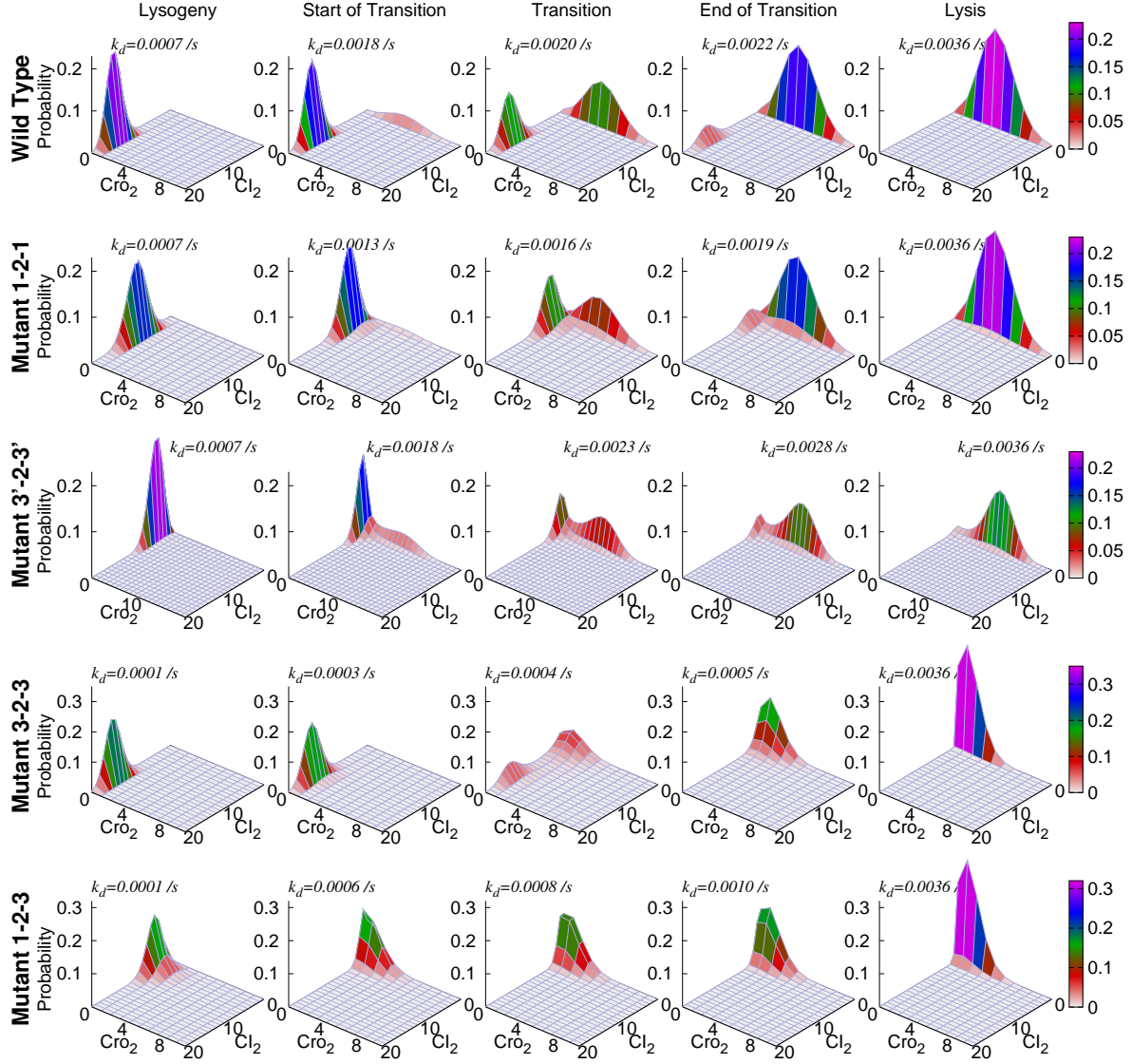


Figure S3: Probability landscapes of wild type, mutant 1-2-1, mutant 3'-2-3', mutant 3-2-3, and mutant 1-2-3 phage lambda at different CI degradation rate k_d .

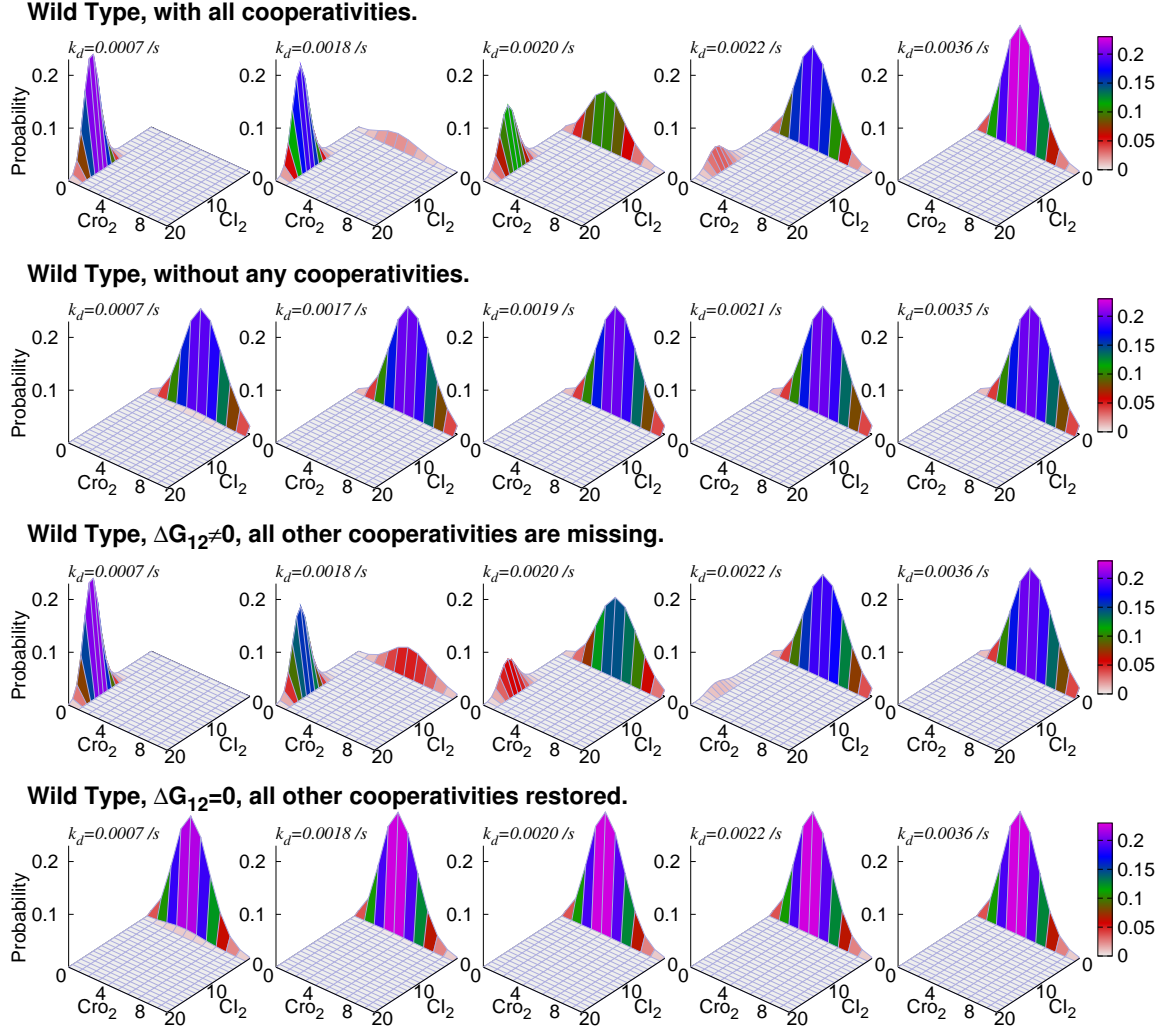


Figure S4: Probability landscapes of wild type phage lambda at different CI degradation rate k_d with all cooperativities intact, all cooperativities removed, with only cooperativity between Cl_2 binding to O_{R1} and O_{R2} restored, and with all but that between Cl_2 binding to O_{R1} and O_{R2} restored.

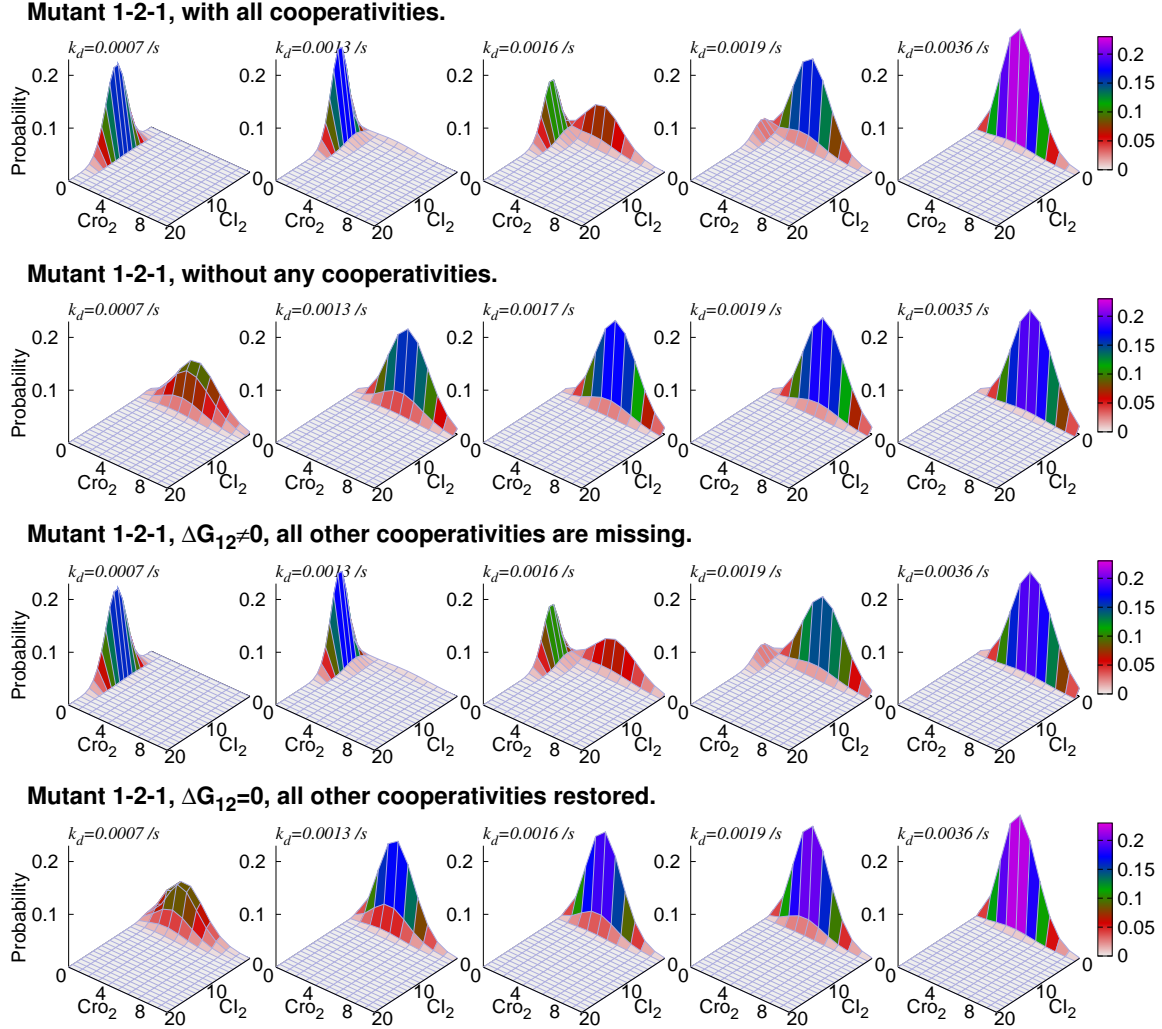


Figure S5: Probability landscapes of mutant 1-2-1 phage lambda at different CI degradation rate k_d with all cooperativities intact, all cooperativities removed, with only cooperativity between Cl_2 binding to O_{R1} and O_{R2} restored, and with all but that between Cl_2 binding to O_{R1} and O_{R2} restored.

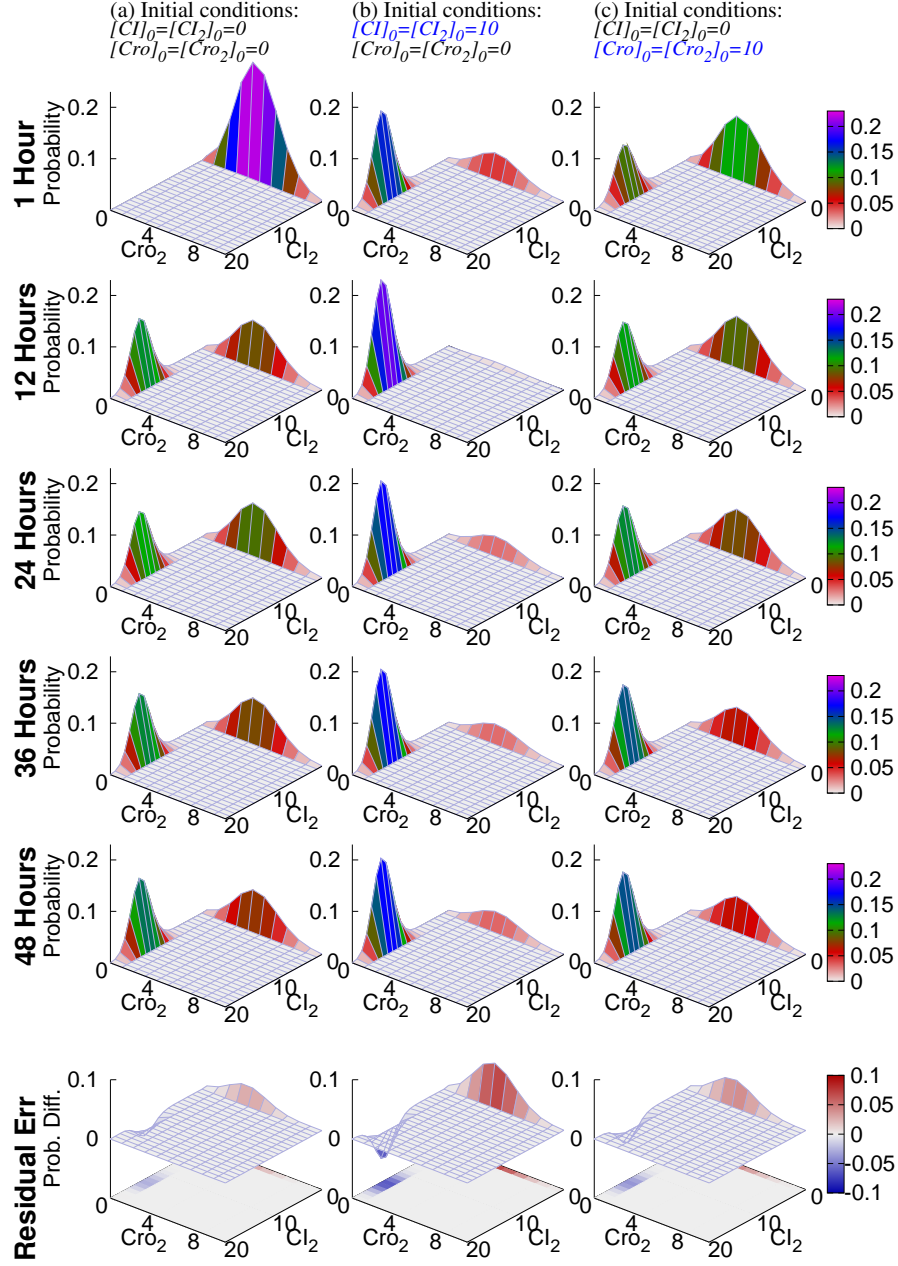


Figure S6: Probability landscape at lysogeny-lysis transition phase ($k_d = 0.0020/s$) computed using stochastic simulation algorithm have not converged after 48 hours when started at different initial conditions. Simulations are run using exactly the same model and parameters for wild-type phage lambda. The true steady state landscape can be seen in the 3rd plot in the first row of Fig. S3. The residual errors between probability landscape distributions obtained from stochastic simulations and the exact solution obtained from dCME are significant after 48 hours of computation (last row).

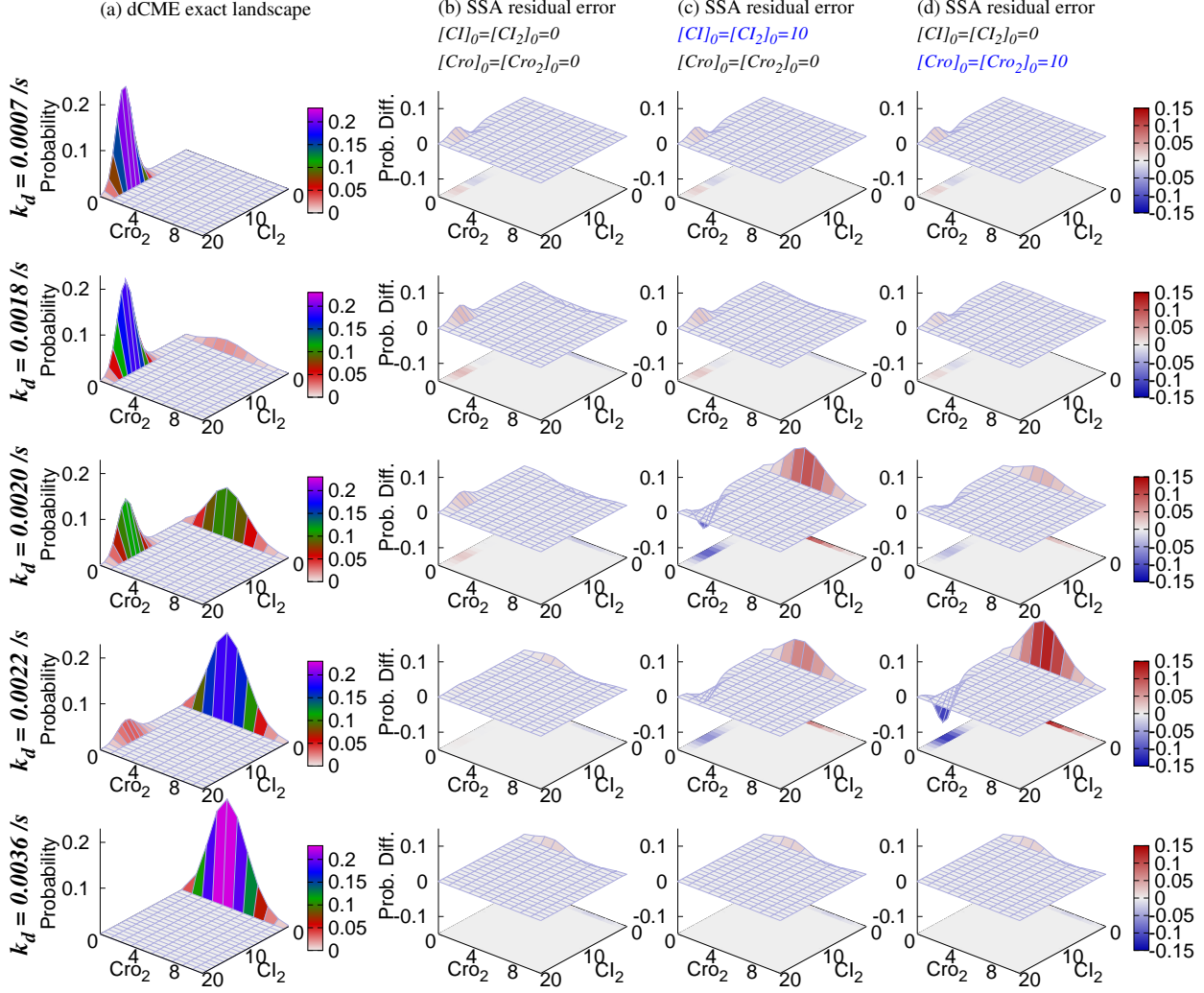


Figure S7: Probability landscape at different regions and corresponding residual errors from SSA simulations after 8 hours. (Left column): The probability landscape from dCME in the lysogenic region ($k_d = 0.0007/s$), at the beginning of the transition region ($k_d = 0.0018/s$), at the transition region ($k_d = 0.0020/s$), at the end of the transition region ($k_d = 0.0022/s$), and in the lytic region ($k_d = 0.0036/s$) are plotted. (Right 3 columns): Residual error from stochastic simulation algorithm with three different initial conditions. For ease of visualization, we plot $P_{\text{dCME}}(x) - P_{\text{SSA}}(x)$ projected onto the $[Cl_2]$ - $[Cro_2]$ space.

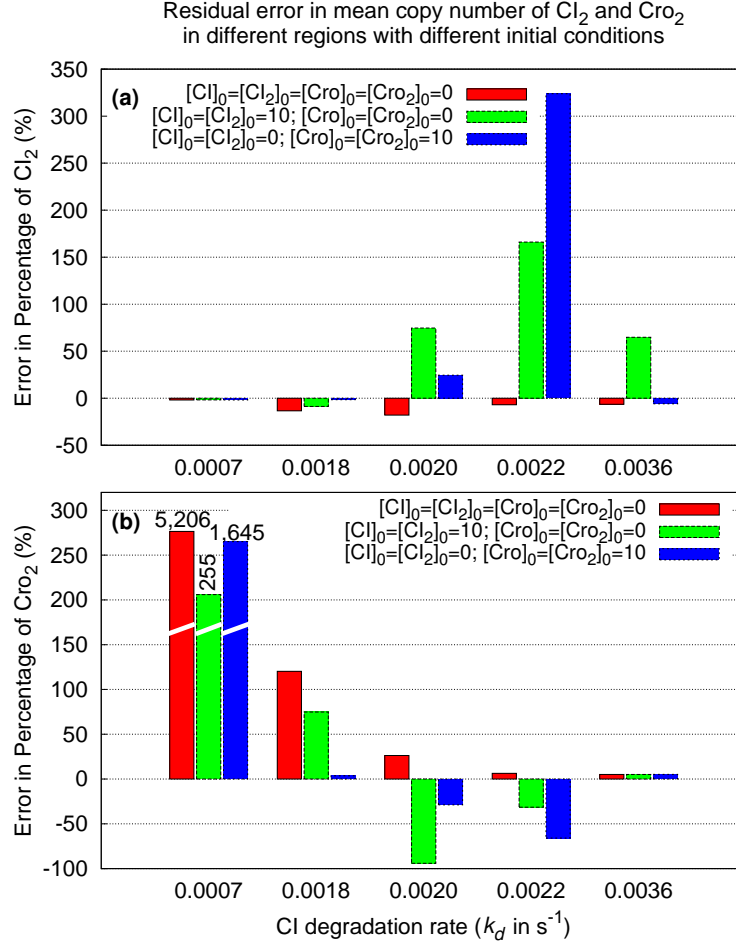


Figure S8: Errors in estimated mean copies of Cl_2 and Cro_2 from SSA simulations at different regions and different initial conditions. (a) Error in estimated copy numbers of Cl_2 ($\mathbb{E}[Cl_2]^{SSA} - \mathbb{E}[Cl_2]^{dCME}) / \mathbb{E}[Cl_2]^{dCME}$ in percentage. (b) Error in estimated copy numbers of Cro_2 ($\mathbb{E}[Cro_2]^{SSA} - \mathbb{E}[Cro_2]^{dCME}) / \mathbb{E}[Cro_2]^{dCME}$ in percentage.

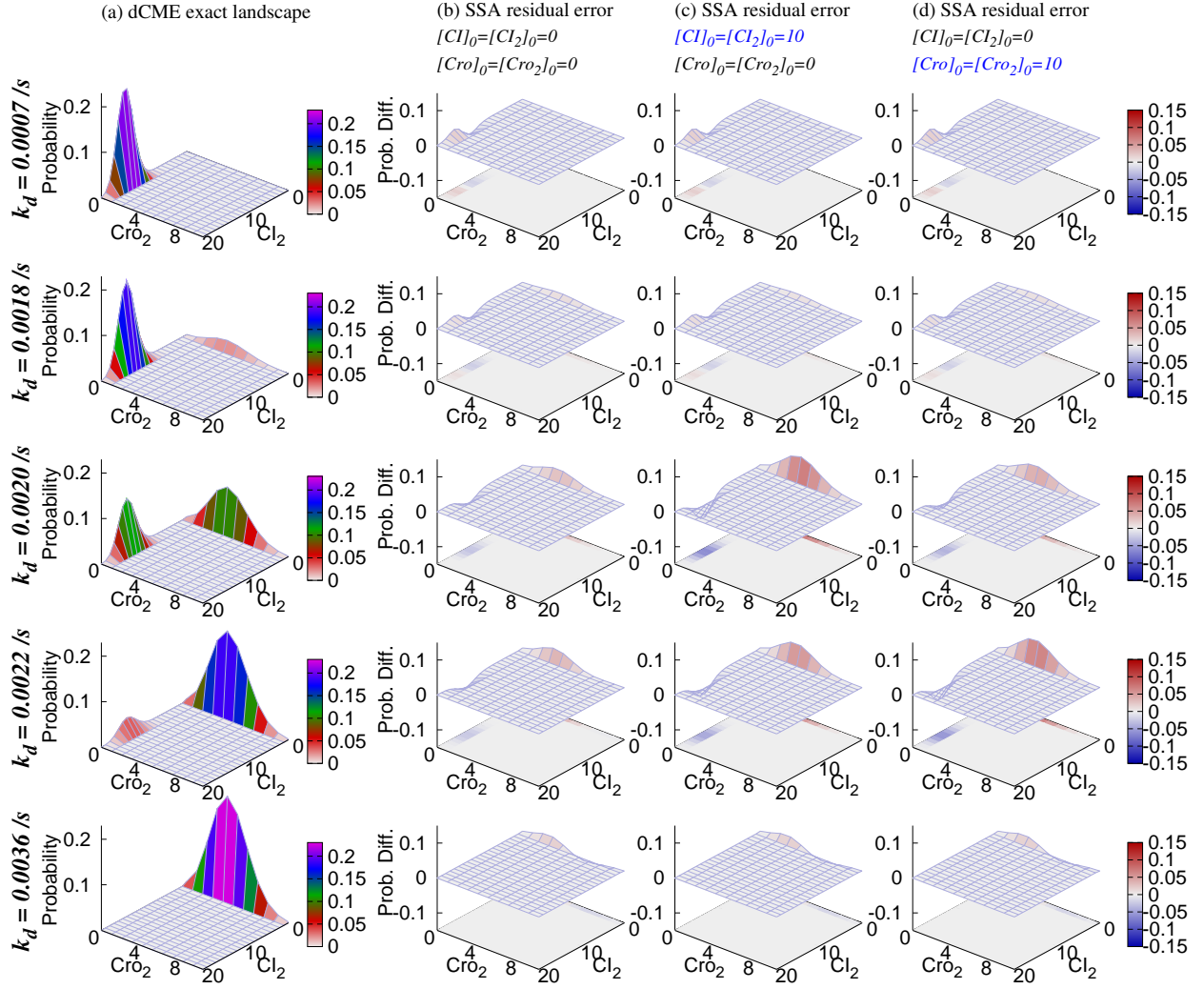


Figure S9: Same as Fig S7 but with SSA simulations after 48 hours.

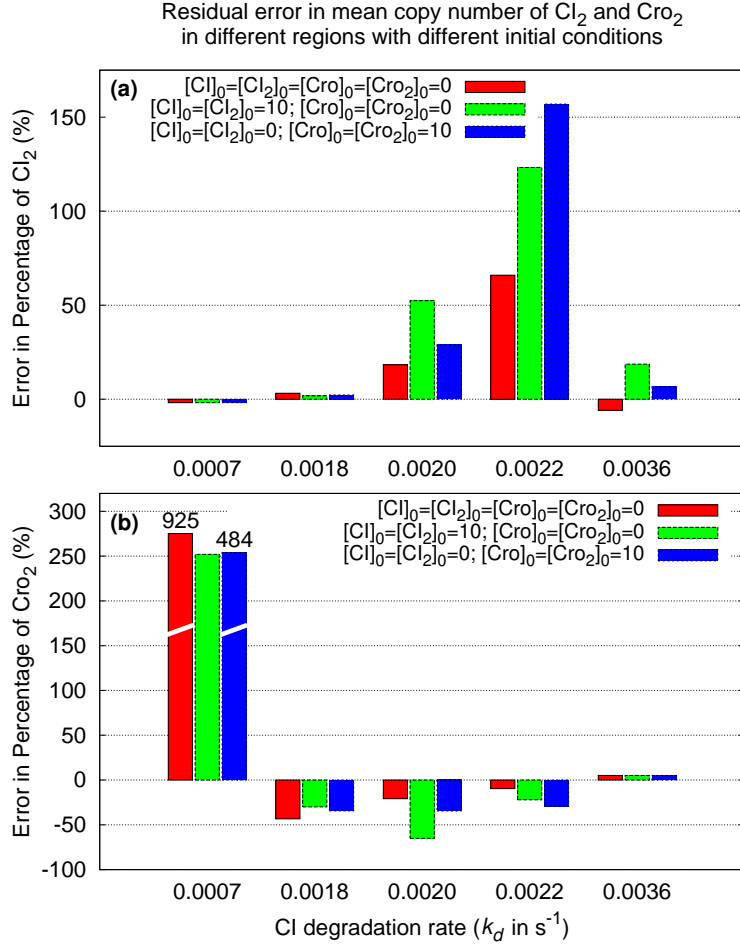


Figure S10: Same as Fig S8 but with SSA simulations after 48 hours.

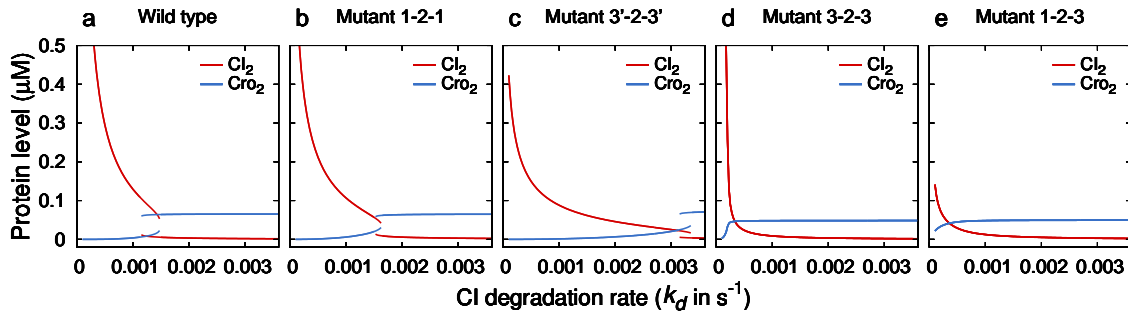


Figure S11: Bifurcation curves of the deterministic model for wild-type phage lambda and the Little's mutants. The deterministic model was based on the formulation of the model from [25], and was built using the same parameters as in the chemical master equation model [27]. Red lines represent the concentrations of Cl_2 in steady state for different CI degradation rates, and the blue lines represent that of Cro_2 in steady state.

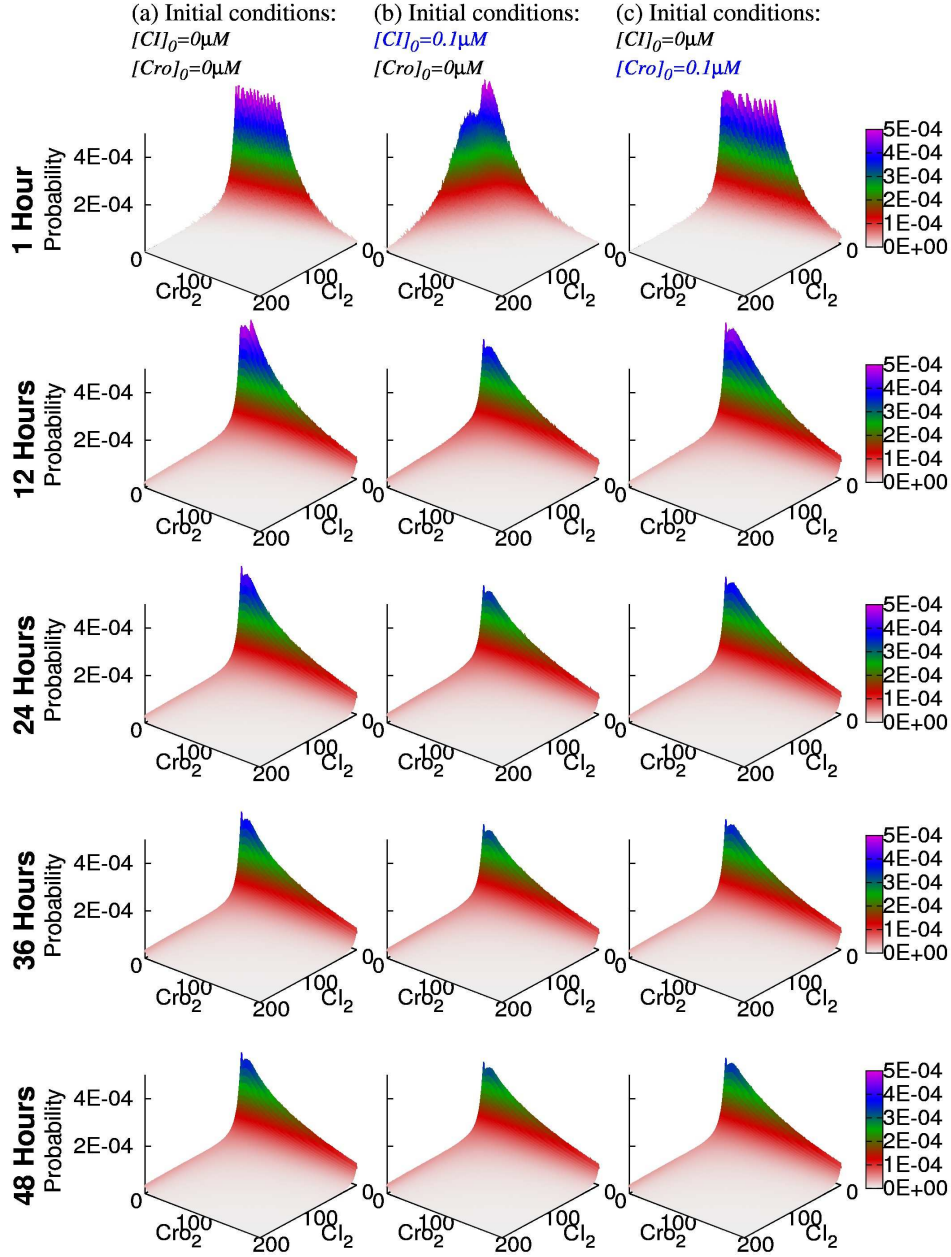


Figure S12: Probability landscape at lysogeny-lysis transition phase ($k_d = 0.0020/s$) computed using stochastic differential equations (SDE) have not converged after 48 hours when started at different initial conditions, and is further away from steady state than results from stochastic simulation. SDE model is built according to the convention of chemical Langevin equation [10] by adding Gaussian noises to ODE model.

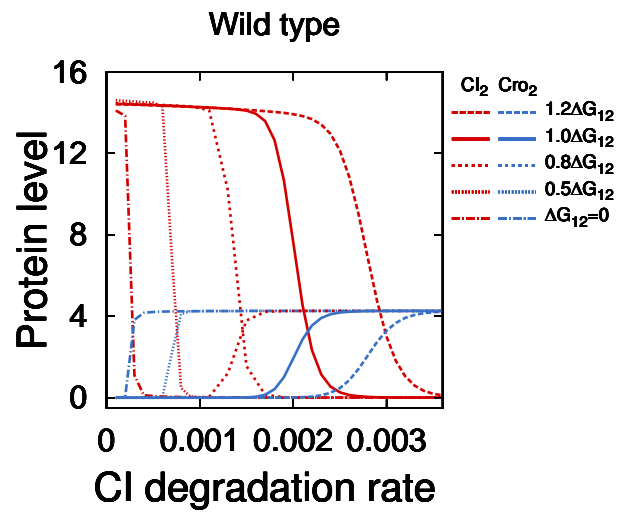


Figure S13: Changes in the binding cooperativity between Cl dimers on O_{R1} and O_{R2} shifts the switching threshold, while the lysogens remain stable. Red lines represent the amounts of Cl_2 , and blue lines the amount of Cro_2 . Solid lines, long dashed lines, short dashed lines, dotted lines, and dash-dot lines stand for the ΔG_{12} modified by a factor of 1.0, 1.2, 0.8, 0.5 and 0.0, respectively.